The enigma of Oligocene climate and global surface temperature evolution

Charlotte L. O'Brien[a,b,1], Matthew Huber[c], Ellen Thomas[a,d], Mark Pagani[a], James R. Super[a], Leanne E. Elder[a,e], and Pincelli M. Hull[a]

[a]Department of Geology and Geophysics, Yale University, New Haven, CT 06511; [b]UCL Department of Geography, University College London, London WC1E 6BT, United Kingdom; [c]Department of Earth, Atmospheric and Planetary Sciences, Purdue University, West Lafayette, IN 47907; [d]Department of Earth and Environmental Sciences, Wesleyan University, Middletown, CT 06459; and [e]Museum of Natural History, University of Colorado, Boulder, CO 80309

Edited by Pierre Sepulchre, Laboratoire des Sciences du Climat et de l'Environnement, Gif sur Yvette, France, and accepted by Editorial Board Member Jean Jouzel August 16, 2020 (received for review March 3, 2020)

Falling atmospheric CO_2 levels led to cooling through the Eocene and the expansion of Antarctic ice sheets close to their modern size near the beginning of the Oligocene, a period of poorly documented climate. Here, we present a record of climate evolution across the entire Oligocene (33.9 to 23.0 Ma) based on TEX_{86} sea surface temperature (SST) estimates from southwestern Atlantic Deep Sea Drilling Project Site 516 (paleolatitude ∼36°S) and western equatorial Atlantic Ocean Drilling Project Site 929 (paleolatitude ∼0°), combined with a compilation of existing SST records and climate modeling. In this relatively low CO_2 Oligocene world (∼300 to 700 ppm), warm climates similar to those of the late Eocene continued with only brief interruptions, while the Antarctic ice sheet waxed and waned. SSTs are spatially heterogenous, but generally support late Oligocene warming coincident with declining atmospheric CO_2. This Oligocene warmth, especially at high latitudes, belies a simple relationship between climate and atmospheric CO_2 and/or ocean gateways, and is only partially explained by current climate models. Although the dominant climate drivers of this enigmatic Oligocene world remain unclear, our results help fill a gap in understanding past Cenozoic climates and the way long-term climate sensitivity responded to varying background climate states.

Eocene–Oligocene | sea surface temperatures | proxy reconstructions | climate models | TEX86

Continental-scale polar ice sheets first reached sea level around Antarctica during the Eocene–Oligocene transition (EOT) (∼34 to 33 Ma) (1, 2). The extent of polar continental ice has been considered so emblematic of the climate state that global climate is commonly described as falling into one of two states: "greenhouse climates," lacking extensive polar continental glaciation (e.g., Paleocene and Eocene climate), and "icehouse climates," with continental polar glaciation (i.e., the Oligocene and younger climate states), with a possibly intermediate late Eocene phase sometimes called the "doubthouse" (3, 4).

However, a simple transition to an icehouse climate and near-modern CO_2 levels across the EOT and separation of Cenozoic climate into two possible states, as commonly proposed, is difficult to reconcile with oxygen isotope ($\delta^{18}O$) values in deep-sea benthic foraminifera that indicate oscillations in deep-sea (thus high-latitude surface) temperature and/or Antarctic ice volume in the Oligocene (e.g., refs. 5–7). Most benthic $\delta^{18}O$ records show an ∼0.5‰ decrease in the late Oligocene (e.g., refs. 5, 6), with warming supported by Mg/Ca (8) and biotic records (9–12), suggesting that late Oligocene deep-water temperatures were close to those in the late Eocene.

Two not mutually exclusive drivers have been proposed to explain Cenozoic temperature trends: changes in ocean gateways and changes in atmospheric CO_2 levels. Ocean gateway changes have long been put forward as an explanation of the major climate changes in the Cenozoic (13–20), but the exact timing of various gateway openings continues to be the subject of ongoing controversy. Climate modeling consistently shows that paleogeography explains only a minor component of the major Cenozoic climate changes (13–21) but may be important for regional sea surface temperature (SST) shifts. Changes in atmospheric CO_2 levels have proven a more plausible explanation of global Cenozoic cooling (22, 23). Reconstructions based on marine proxies show that CO_2 concentrations declined from ∼1,000–800 to ∼700–600 ppm across the EOT (24–27) (Table 1). This drop, in combination with orbital variability (28, 29), may have initiated unipolar Antarctic glaciation.

What happened next is less clear. CO_2 may have increased again to ∼1,000 ppm from 30 to 29 Ma, then declined from ∼700 to 300 ppm during the late Oligocene (26, 33, 34) (Table 1), but the data have large uncertainties (26). Leaf stomatal and leaf gas exchange model proxy data show late Eocene CO_2 values of ∼400 ppm, generally slightly increasing from the late Oligocene into the early Miocene (32, 35, 36), with a large spread of possible values in the early Miocene (∼300 to 1,300 ppm) (37). Regardless of the exact trends, proxy records indicate that Oligocene CO_2 values were, on average, lower than Eocene values (<800 ppm), notably approaching modern/preindustrial values (∼300 ppm) during the interval termed "late Oligocene warming" (LOW) (∼26.5 to 24 Ma) (10, 38).

We know relatively little about Oligocene climate. Marine and terrestrial surface temperature reconstructions are temporally restricted and spatially sparse, and mostly concentrated on southern high latitudes (e.g., ref. 39) and the EOT (e.g., refs. 40,

Significance

During the Eocene, high-latitude regions were much warmer than today and substantial polar ice sheets were lacking. Indeed, the initiation of significant polar ice sheets near the end of the Eocene has been closely linked to global cooling. Here, we examine the relationship between global temperatures and continental-scale polar ice sheets following the establishment of ice sheets on Antarctica ∼34 million years ago, using records of surface temperatures from around the world. We find that high-latitude temperatures were almost as warm after the initiation of Antarctic glaciation as before, challenging our basic understanding of how climate works, and of the development of climate and ice volume through time.

Author contributions: C.L.O., M.H., and M.P. designed research; C.L.O., M.H., and L.E.E. performed research; C.L.O., M.H., E.T., J.R.S., and P.M.H. analyzed data; and C.L.O., M.H., E.T., J.R.S., and P.M.H. wrote the paper.

The authors declare no competing interest.

This article is a PNAS Direct Submission. P.S. is a guest editor invited by the Editorial Board.

[1]To whom correspondence may be addressed. Email: c.l.obrien@ucl.ac.uk.

This article contains supporting information online at https://www.pnas.org/lookup/suppl/doi:10.1073/pnas.2003914117/-/DCSupplemental.

First published September 28, 2020.

Table 1. CO_2 proxy estimates, from alkenones, marine boron, coccoliths, and leaf stomata, for Eocene–Oligocene time slices

Time slice	Proxy-derived pCO_2, ppm						References
	Mean	Median	Min	Max	Min (inc. error)	Max (inc. error)	
40–33.9 Ma	979	947	365	2,622	270	3,212	Ref. 30 and references therein; ref. 31
33.9–33 Ma	783	767	409	1,088	303	1,234	Ref. 30 and references therein; ref. 31
33–26.5 Ma	705	726	391	972	317	1,179	Ref. 30 and references therein; refs. 31, 32
25–23.5 Ma	298	259	222	476	166	600	Ref. 30 and references therein; refs. 33, 34

41). In the absence of adequate surface temperature records, the climate of the Oligocene has been indirectly inferred from benthic oxygen isotope records (42). This method can lead to large biases as it assumes nonchanging vertical ocean temperature stratification, likely a poor assumption (15, 17, 18).

Here, we provide ∼100-ky resolution SST reconstructions of the Oligocene–lowermost Miocene (∼32 to 22 Ma) western subtropical and tropical Atlantic, using the TEX_{86} paleothermometer at southwestern Atlantic Deep Sea Drilling Project (DSDP) Hole 516F and western equatorial Atlantic Ocean Drilling Program (ODP) Hole 929A (Figs. 1 and 2). These sites are among the few with continuous Oligocene–Miocene sediments and good organic matter preservation. Our approach to reconstructing SSTs relies on lipids produced by archaea (TEX_{86}) and haptophyte algae ($U^{k'}_{37}$). These SST proxies are not subject to the diagenetic problems of Late Cretaceous through Miocene planktonic foraminiferal $\delta^{18}O$ values, which may be strongly affected by sea floor recrystallization that can result in underestimated SSTs (e.g., refs. 43, 44).

We combine our data with 1) TEX_{86} records from IODP Site U1404, Newfoundland Margin (North Atlantic; Figs. 1 and 2*A* and ref. 46) and IODP Site U1356 offshore Wilkes Land (East Antarctica; Fig. 2*D* and ref. 39) to resolve global Oligocene SST evolution (Fig. 2), and 2) published paleotemperature proxy records and global climate models, providing a synthesis of Oligocene temperature evolution (Figs. 3 and 4). TEX_{86} values were computed after ref. 49 and converted to SST using the analog BAYSPAR calibration, a Bayesian regression approach designed for applications in "deep time" (47, 48). The fidelity of TEX_{86} as a temperature proxy was assessed using various glycerol dialkyl glycerol tetraether (GDGT) indices: branched and isoprenoid tetraether (BIT), ring index (ΔRI), and methane index (MI) (*Methods* and *SI Appendix*, Text 1).

Tropical–Subtropical TEX_{86} SST Records

TEX_{86} values in Hole 516F range between 0.69 and 0.77, corresponding to TEX_{86}-SSTs of 26.4 to 32.1 °C (Fig. 2*C*) (48). BIT indices (0.04 to 0.28; mean value, 0.13) suggest little input of terrestrial-derived GDGTs (*SI Appendix*, Figs. S1 and S2). MI values are low (0.13 to 0.19), suggesting normal sedimentary conditions, and only one sample records a |ΔRI| value >0.3. In Hole 929A, TEX_{86} values range between 0.67 and 0.79, corresponding to TEX_{86}-SSTs of 25.4 to 33.5 °C (Fig. 2*B*) (48). BIT index values are high (0.32 to 0.97; mean, 0.73; *SI Appendix*, Figs. S1 and S2) but do not appear to significantly influence TEX_{86}-SST estimates, based on comparison with nearby Site 925 (*SI Appendix*, Text 2). Fifty of 81 samples have |ΔRI| values >0.3, potentially indicative of nonthermal influences on the GDGT distributions (57). However, the covariance of |ΔRI| and TEX_{86} is relatively low, $R^2 = 0.24$ ($P = 0.0001$; *SI Appendix*, Fig. S2*B*), and removal of TEX_{86} data associated with |ΔRI| values >0.3 ($n = 50$) does not alter the magnitude or nature of the long-term trends in TEX_{86}-based SSTs (*SI Appendix*, Fig. S4). Thus, we interpret TEX_{86} values as SSTs at Hole 929A (with the exception of one datapoint: see *SI Appendix*, Text 1), with the implication that high BIT values in Hole 929A have little impact on absolute TEX_{86}-SST estimates.

Trends in Oligocene SST

Biomarker-based temperature estimates for four Oligocene locations spanning high to low latitudes (Fig. 2 *A*–*D*) record geographically heterogenous patterns of SST change, although most support relatively cool early Chattian temperatures (∼28.0 to 26.5 Ma), as indicated by benthic isotope records (i.e., Fig. 2*E*). All but the highest latitude SST record indicate late Oligocene (∼26.5 to 24.5 Ma) warming of approximately +1 to 2 °C. Records differ in other features. SSTs at IODP Site U1356 offshore Wilkes Land (East Antarctica; 185-ky resolution; Fig. 2*D*) (39) generally cooled throughout the Oligocene, with an acceleration around 24.5 Ma. This cooling may not be a general feature of the Southern Oceans, since biotic evidence suggests LOW at ODP Sites 738 (Kerguelen Plateau) and 689 (Maud Rise, Weddell Sea) (10).

Regionally heterogenous SSTs characterize the EOT (40, 46) and the late Oligocene (Fig. 2 *A*–*D*). We show model-derived surface temperature estimates from a suite of different model cases spanning a range of plausible CO_2 and ice volume scenarios (Fig. 2 and *SI Appendix*, Table S1) for the four locations. These are, with the exception of Hole 929A, generally cooler than the proxy data, at some sites markedly so (>5 °C cooler; Fig. 2). This data–model offset is more extreme for the early-middle Oligocene compared to the late Oligocene. Modeled surface temperatures at Hole 929A are within the range of proxy data for both the early-middle and late Oligocene, reflecting the generally better proxy–model agreement at low-latitude sites (Fig. 4). Similar to the proxy data, the models on average predict higher SSTs in the late Oligocene than in the early-middle Oligocene at all sites except Hole 929A, where the models indicate minor (∼1 °C) cooling. Thus, the models appear to broadly capture long-term heterogenous trends in Oligocene SST evolution. However, large data–model offsets, especially at higher latitudes, emphasize uncertainties in model reconstructions of Oligocene climates, including the role of various climate forcings

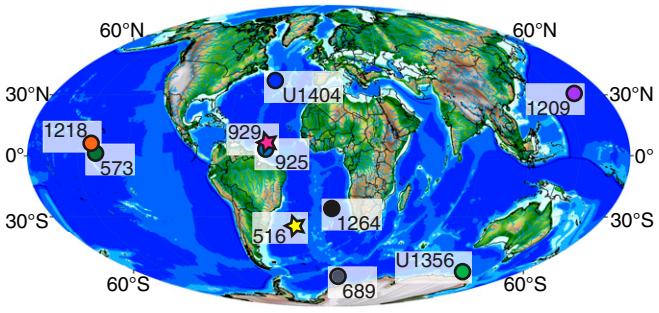

Fig. 1. Paleogeographic reconstruction of the late Oligocene (Chattian). Paleopositions of the study sites (stars; ODP Hole 929A and DSDP Hole 516F) and other sites from which data are discussed in the text and/or presented in Figs. 2 and 3 (circles; DSDP Site 573; ODP Sites 689, 925, 1209, 1218, and 1264; and IODP Sites U1356 and U1404) are indicated. Oligocene paleogeography was provided by Markwick (45).

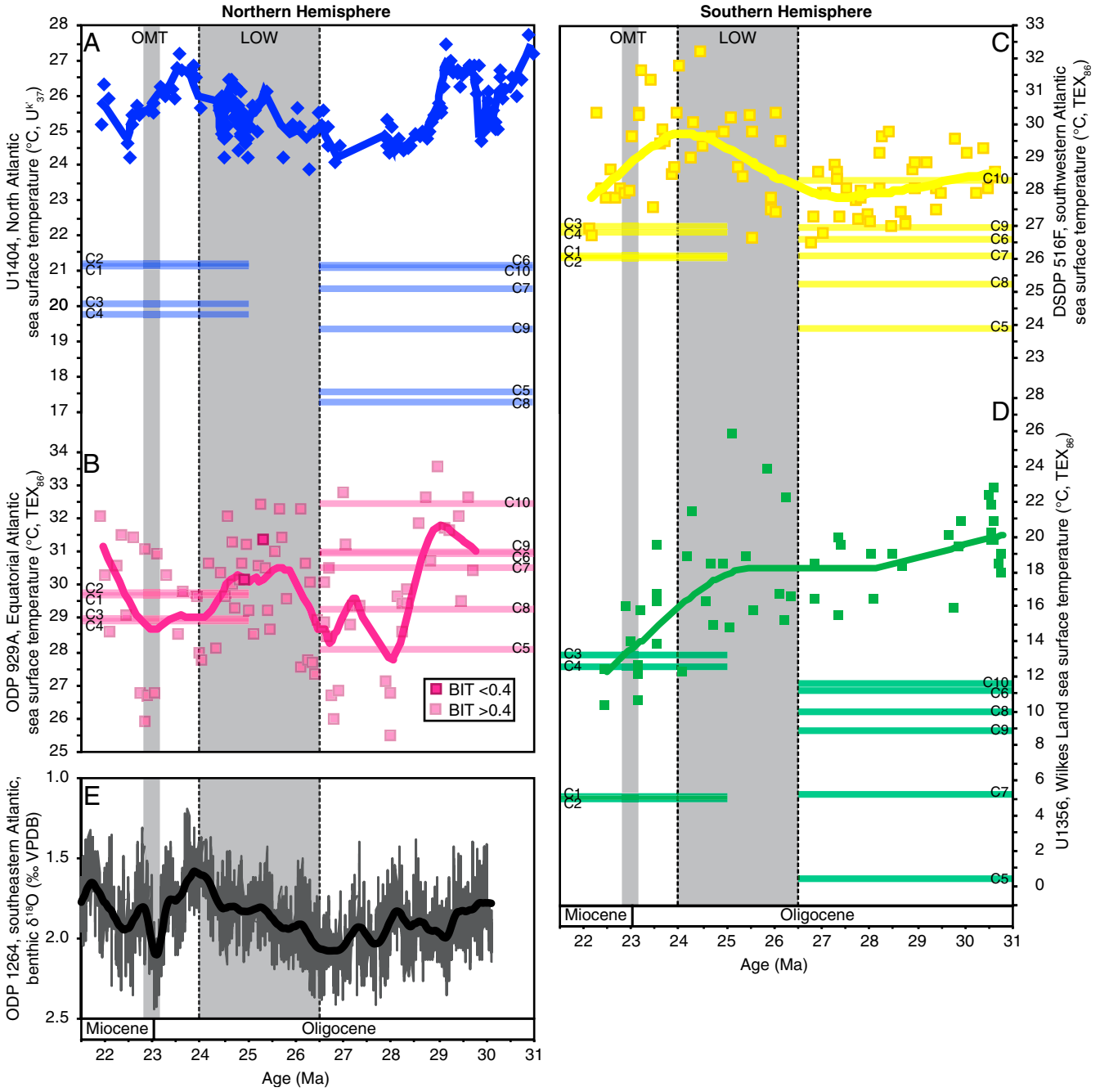

Fig. 2. Middle Oligocene–early Miocene paleoclimate records. (*A*) North Atlantic $U^{k'}_{37}$ SST estimates from IODP Site U1404 (46). (*B*) Tropical Atlantic TEX_{86} SST estimates from ODP Hole 929A (this study). (*C*) Southwestern Atlantic TEX_{86} SST estimates from DSDP Hole 516F (this study). (*D*) TEX_{86} SST estimates from IODP Site U1356 offshore Wilkes Land, Antarctica (39). Note this temperature scale is twice that of *A*–*C*. (*E*) Benthic $\delta^{18}O$ record from ODP 1264 (5). TEX_{86}-SSTs are calculated using the BAYSPAR deep-time calibration (47, 48). Calibration uncertainties for new TEX_{86} data vary between 4 and 8 °C with a median of 6 °C (*SI Appendix*, Fig. S5). The shaded horizontal bars in *A*–*D* represent model-derived surface temperature estimates for the middle Oligocene and late Oligocene–early Miocene for a suite of different model cases, C1–10. Details of model cases are given in *SI Appendix*, Table S1. Temperature and benthic oxygen isotope data are fitted with a LOESS model (thick lines). LOW, late Oligocene warming; OMT, Oligocene–Miocene transition.

such as concentrations of greenhouse gases and boundary conditions such as global ice volume.

Similarly, LOW is generally supported by the proxy records but cannot easily be reconciled with sparse evidence for declining CO_2 throughout the Oligocene (26) (Figs. 2 and 3*F* and Table 1). Additional CO_2 estimates from a range of proxies at higher temporal resolution are needed to constrain Oligocene CO_2 concentrations. CO_2 must have declined at some time in the Oligocene, following the rebound after the EOT, suggesting that non-CO_2 factors such as reduced (relative to the EOT) Arctic sea ice (15, 58, 59), Antarctic ice sheet and climate interaction, and cloud feedbacks may have been important in regulating global mean temperatures.

Oligocene Surface Temperature Evolution

We use our tropical Atlantic SST record from Hole 929A (Fig. 2*B*) to extend the Eocene tropical SST compilation from ref. 23 through the Oligocene (Fig. 3*B*). Surprisingly, our

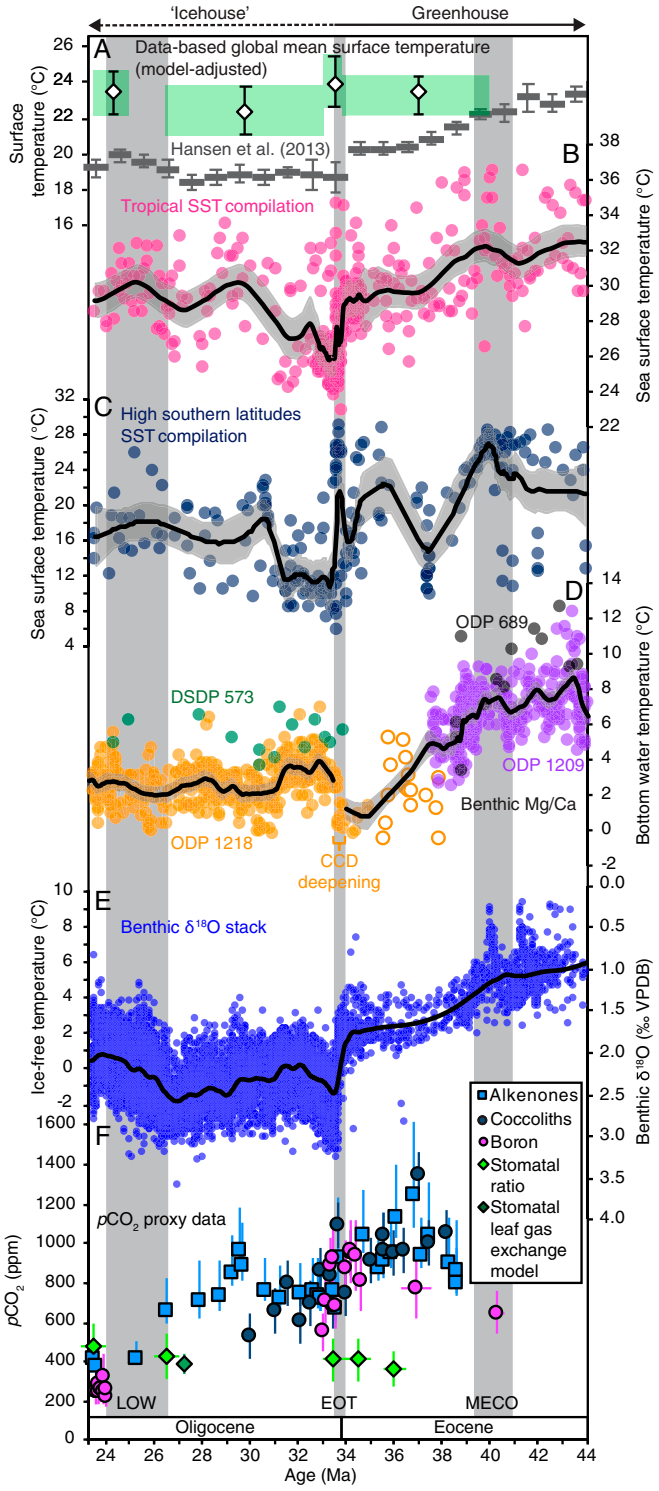

Fig. 3. Eocene–Oligocene temperature and climate evolution. (*A*) Data-based GMST estimates (model-adjusted; this study) and previous benthic δ^{18}O-derived surface temperature estimates of ref. 42 in 1-My bins; (*B*) tropical SST compilation (this study, ref. 31, and ref. 23 and references therein); (*C*) high southern latitudes SST compilation (refs. 39, 40, 50–54, and ref. 16 and references therein); (*D*) benthic *Oridorsalis umbonatus* Mg/Ca temperature estimates (8, 55, 56); unfilled data points with an orange border are from ODP Site 1218, possibly with diagenetic alteration (8); (*E*) benthic oxygen isotope compilation (refs. 1, 5, and ref. 23 and references therein); (*F*) proxy data CO_2 estimates from alkenones (26, 34), coccoliths (31), marine boron (24, 27, 30, 33), and leaf stomatal ratios (35) and a stomata leaf gas exchange model (32). One alkenone data point (2,622 ppm at 36.48 Ma; ref. 26) was omitted for scaling purposes. Temperature and benthic oxygen isotope data are fitted with a LOESS model (black lines; *SI Appendix*, Text 4.7) and 95% confidence interval (gray shading). CCD, carbonate compensation depth; EOT, Eocene–Oligocene transition; LOW, late Oligocene warming; MECO, middle Eocene climatic optimum.

compilation indicates that in the late Oligocene (~26 to 24 Ma), a time typically thought to have been characterized by an icehouse climate, tropical SSTs were as warm as those in the greenhouse climate of the late Eocene (Fig. 3 *A* and *B*). This previously unrecognized similarity in surface temperatures is supported by late Oligocene benthic δ^{18}O values approaching late Eocene values of ~1.5 to 2‰ (Fig. 3*E*) (1). Late Oligocene high southern latitude SSTs are also within the range of middle–late Eocene SST reconstructions from these regions, although the data are more variable (Fig. 3*C*).

To develop a global picture of climate evolution across the Oligocene, and to assess its warmth relative to the better characterized Eocene, we compiled multiple surface temperature proxy records. To evaluate whether the observed patterns of global warmth and apparently anomalous warm polar temperatures could be explained with known forcing factors (e.g., paleogeography, pCO_2, etc.), we compared the resulting surface temperature compilation against two suites of climate model simulations for four time slices: 1) 40.0 to 33.9 Ma, the late Eocene; 2) 33.9 to 33.0 Ma, the earliest Oligocene; 3) 33.0 to 26.5 Ma, the early-middle Oligocene; and 4) 25.0 to 23.5 Ma, the late Oligocene (Fig. 4 and *SI Appendix*, Fig. S9). Oligocene multiproxy data indicate persistent surface warmth for these time slices (Fig. 4 and *SI Appendix*, Fig. S9), with Oligocene latitudinal surface temperature gradients significantly lower than those of today.

To establish whether these patterns agree with expectations from physical models, we compared them with results from two sets of modeling experiments using the NCAR CESM1.0 and the UK HADCM3L model. The NCAR CESM1.0 simulations have been well-characterized in a series of studies spanning a range of plausible Eocene–Oligocene CO_2 scenarios (400, 560, 840, and 1,120 ppm) and boundary conditions (*Methods*). To complement these simulations, we compared the results with those of simulations with the HADCM3L model (60), which has more accurate and refined representations of the paleogeography through the Oligocene. We performed model–data comparisons separately for each model and time slice, then generated ensemble mean model–data anomalies for each model. Despite the use of two very different models with substantially different boundary conditions, the model–data discrepancy is robust and nearly stationary. Throughout the Oligocene, equator–pole surface temperature gradients are smaller than modern, and models cannot simultaneously reproduce proxy-derived tropical and high-latitude SSTs (Fig. 4). This mismatch, which we show here for the Oligocene, resembles the persistent model–data discrepancies in the Eocene (24, 61, 62) and early Miocene (63).

The models consistently underestimate high-latitude warming and produce steeper latitudinal surface temperature gradients than in proxy reconstructions (Fig. 4 and *SI Appendix*, Fig. S9) or model simulations for the late Eocene (23) (*SI Appendix*). We employed the same model, CESM1.0, as Cramwinckel et al. (23), who argued that the model reproduced the Eocene proxy data temperature gradient, but we do not observe this for the Oligocene—a different time period for which the range of paleogeographies is smaller, and trends in middle- and high-latitude SST proxy estimates are less equivocal (*SI Appendix*, Text 6). The proxy data–model offset is more extreme under lower than under higher CO_2 scenarios (400 and 560 ppm), and in simulations with rather than without Antarctic glaciation.

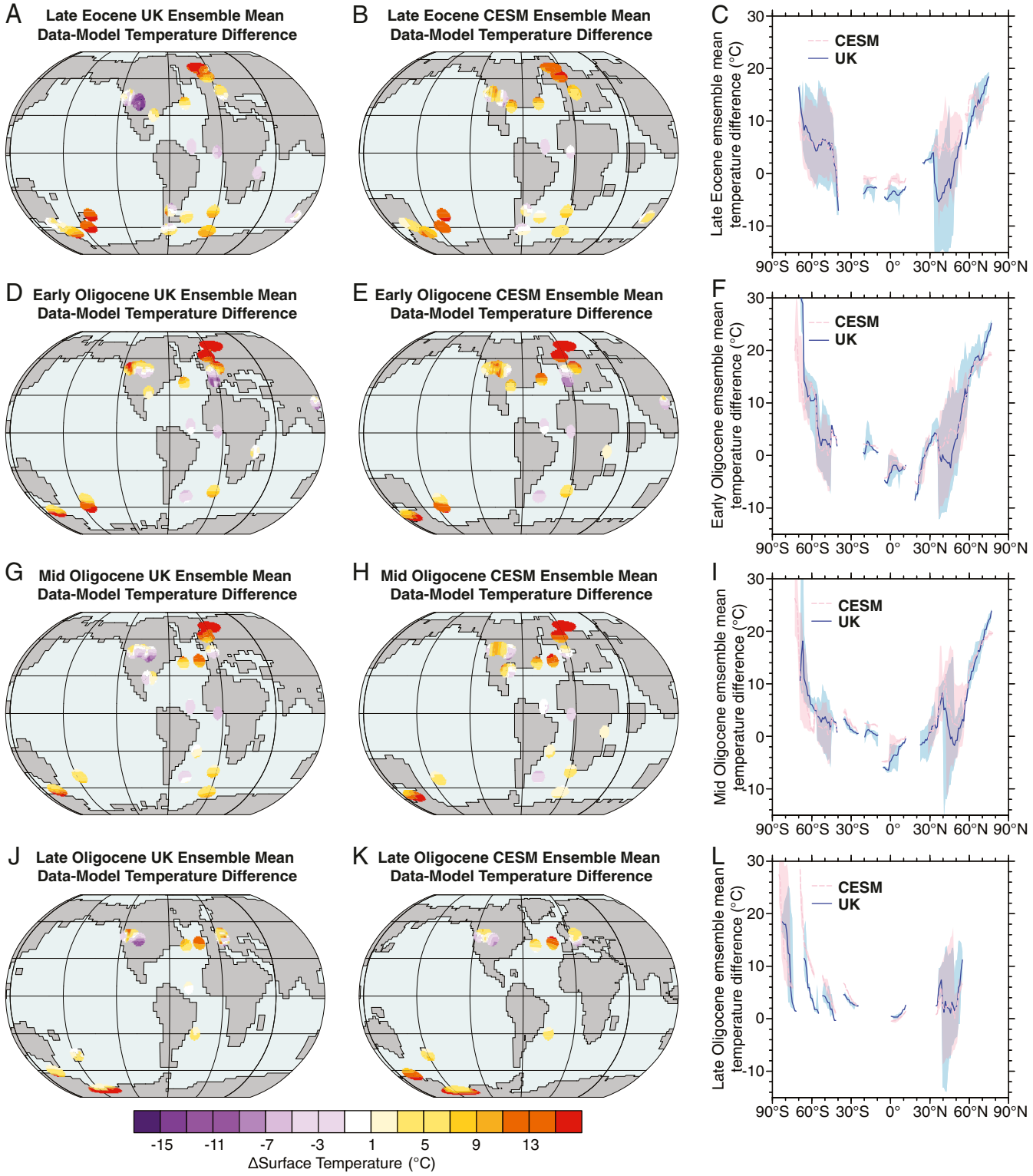

Fig. 4. Eocene–Oligocene surface temperature data–model comparisons. (*A*–*L*) Surface temperature data–model comparisons for four Eocene–Oligocene time slices. Data–model comparisons are represented both spatially (*A*, *B*, *D*, *E*, *G*, *H*, *J*, and *K*) and as zonal mean of the differences versus latitude (*C*, *F*, *I*, and *L*). Differences in *A*, *B*, *D*, *E*, *G*, *H*, *J*, and *K* are calculated as the pointwise difference between the proxy mean value and model annual mean, then optimally interpolated and plotted as "circles" of difference. The shaded bands in *C*, *F*, *I*, and *L* represent minimum and maximum differences associated with the zonal means. Proxy data were compared to ensembles means from HadCM3L (UK) and CESM simulations. Modeling details are provided in *SI Appendix*, Table S1. Compiled Eocene–Oligocene surface temperature proxy data are shown in *SI Appendix*, Fig. S9. Refer to *Methods* and *SI Appendix*, Text 5, for further details.

Progress has been made in simulating high-latitude warmth for the early Eocene (64) and Pliocene (65, 66), through incorporation of cloud microphysics feedbacks. Ref. 64 represents an important advance in simulating higher early Eocene global mean surface temperature (GMST) estimates under less extreme CO_2 conditions. Similarly, improvements in modeling resolution for the late Eocene (67) and EOT (21) provide a significant step forward in resolving ocean geography, gateways, and circulation. However, further investigations are still required since the long-term stability of these simulations is questionable, and the model–data biases in the latitudinal surface temperature gradient remain unsolved (*SI Appendix*, Text 5.2).

We use our Oligocene surface temperature compilation to estimate GMST directly, after Caballero and Huber (68) (see *SI Appendix*, Text 4.2, for method details; Fig. 3*A*). Oligocene GMSTs were ∼22 to 24 °C (Fig. 3*A*), thus not significantly different from those of the late Eocene, 23 °C, and >8 °C higher than modern rather than ∼5 °C (e.g., refs. 42, 69). We therefore do not reconstruct clearcut differences in surface temperature conditions between the late Eocene (greenhouse world) and the Oligocene (icehouse world) after its earliest glaciation.

This significant upward revision of GMSTs requires a reevaluation of estimates of climate sensitivity (42, 69, 70). If there are no unidentified issues with current Eocene–Oligocene CO_2 estimates and/or collective biases in multiproxy surface temperature records, a commensurate increase in climate sensitivity estimates may be necessary, unless an as-yet-unidentified non-CO_2 forcing can be found. For example, geographically static biases on proxy reconstructions, whether due to seasonal cycles, regional diagenesis, and/or other environmental controls, could result in similar net temperature biases across different proxy systems in a given region. If current multiproxy surface temperature reconstructions are valid, their high-latitude warmth requires rethinking of the stability of Antarctic glaciation in a warmer world (71). The fact that ice volume remained large after the EOT even as the world returned to a warm state similar to that in the late-middle Eocene suggests an important role for hysteresis, changes in topography and elevation (e.g., ref. 72), or fluctuations in ice volume without warming.

Enigmatic Oligocene Climate State

Multiple-proxy Oligocene surface temperature records document consistent warmth at higher latitudes (Figs. 3*C* and 4), which is, at first glance, difficult to reconcile with the presence of 1) a relatively cool deep ocean (Fig. 3*D*), 2) Southern Hemisphere ice, and 3) climate models. However, in some model simulations, Antarctic glaciation leads to regional warming (73, 74), which may partially explain the proxy records. Other models indicate that Antarctic glaciation should lead to preferential cooling of the deep ocean and the high-latitude Southern Ocean and North Atlantic, but this is difficult to reconcile with our compilation (15, 75). Alternatively, the multiproxy data could be collectively biased, for example skewed to the warm season (76). This issue warrants further investigation, but if we take Oligocene surface temperature records at face value, we conclude that warm, low-gradient climates characterized nearly the entire Paleogene. This implies that either the timing and extent of deep-water connections between the Pacific and Atlantic Oceans, used to explain Eocene high-latitude warmth (77–79), occurred much later than commonly argued (i.e., in the Miocene) (80, 81), or they did not cause high-latitude Eocene warmth.

These proxy records and climate model simulations agree with an emerging view (i.e., ref. 82) that Oligocene climate was distinct from the bipolar-glaciated, late Neogene icehouse world and was characterized by warm surface temperatures similar to those in the low-ice late Eocene greenhouse world. This "enigmatic Oligocene" climate state of the Cenozoic was defined by relatively warm global mean temperatures, flattened meridional temperature gradients, and the presence of Antarctic continental ice sheets. From an ecological perspective, the importance of these enigmatic climates is underscored by the fact that the boundary between the Paleogene and Neogene Periods, based on similarity between biota, is placed between the Oligocene and Miocene epochs, and not at the EOT greenhouse/icehouse division (83, 84). From a climatic perspective, the existence of these enigmatic climates highlights critical gaps in our understanding of past climate states, including the way in which factors such as ocean circulation and cloud feedbacks (15) can support sustained global warmth even in the presence of extensive polar continental ice, and possibly relatively low CO_2 concentrations.

Methods

Sampling Strategy. ODP Hole 929A [Fig. 1; 5°58.573′N, 43°44.396′W; 4356 m; paleolatitude ∼0° (85)] is in the western equatorial Atlantic on Ceara Rise. DSDP Hole 516F [Fig. 1; 30°16.590′S, 35°17.100′W; present water depth, 1,313 m; paleolatitude ∼36°S (85)] is in the South Atlantic subtropical gyre on the northern flanks of the Rio Grande Rise. Lower Oligocene to lowermost Miocene (30 to 22 Ma) marine sediments from both sites were sampled at ∼100-ky resolution, analyzing 81 samples from Hole 929A (304.02 to 446.09 mbsf), 81 from Hole 516F (129.66 to 472.86 mbsf). Sample ages were linearly interpolated from surrounding age datums, assuming a constant sedimentation rate. The age model for Hole ODP 929A is after ref. 25 and references therein. For Hole 516F, the age model above 259.5 mbsf is based on magnetostratigraphy (86) with biostratigraphic datums from ref. 87. Below 264 mbsf, ages are constrained by biostratigraphic datums (87, 88). All ages are reported on the Geologic Time Scale 2012 (84) (GTS2012).

GDGT Biomarker Analysis. GDGTs were measured in lipid polar fractions. Lipids were extracted from freeze-dried, manually powdered sediments using a Dionex Accelerated Solvent Extractor 300 with a solvent mixture of dichloromethane (DCM)/methanol (MeOH) (2:1 [vol/vol]). Total lipid extracts were separated into apolar (archived) and polar fractions using alumina column chromatography, eluting with Hexane/DCM (9:1 [vol/vol]; for apolar hydrocarbons) and DCM:MeOH (1:2 [vol/vol]; for polar compounds including GDGTs) (89). Polar fractions were dried under N_2, redissolved in hexane/isopropanol (99:1 [vol/vol]), and then passed through a 0.45-μm polytetrafluoroethylene filter prior to analysis. Isoprenoidal and branched GDGTs were measured on an Agilent 1200 high-performance liquid chromatography/mass spectrometry (HPLC/MS) system at Yale University. Compound separation was achieved using two ultra-high performance liquid chromatography silica columns (Waters BEH HILIC columns, 2.1 × 150 mm, 1.7 μm) in series, fitted with a precolumn of the same material (90). GDGTs were detected following HPLC/MS settings in ref. 89. TEX_{86} values were computed after ref. 49 and converted to SST using the analog BAYSPAR calibration. The BAYSPAR deep-time model provides a more statistically robust assessment of calibration uncertainty than traditional TEX_{86} calibrations, avoids regression dilution bias, and is targeted to geological applications (47). To monitor potential non-SST effects on GDGT distributions, branched and isoprenoidal GDGT measurements were used to compute additional GDGT indices [the BIT index (91), the MI (92), and the ΔRI (57)].

Climate Modeling. We present long, fully coupled integrations of the NCAR CESM1.0.5 using the CAM4 atmosphere, with simulations largely published: the late Eocene and early to middle Oligocene simulations were performed at the T31 atmospheric and ×3° nominal ocean resolution (15, 23) and with atmospheric CO_2 levels of 560 and 1,120 ppm with varying glaciation conditions. The late Oligocene simulation is adapted from the early to middle Miocene boundary conditions of refs. 15, 93, 94, at atmospheric CO_2 levels of 400 ppm, at the 2° nominal atmospheric and ×1° ocean resolutions, and with some small ocean gateway changes appropriate for the late Oligocene (but otherwise preindustrial atmospheric boundary conditions). A range of gateway changes were tested to explore sensitivity to the likely changes in boundary conditions between the early Miocene and late Oligocene, specifically as to the depth of the Greenland–Scotland Ridge (95). Model conditions are detailed in *SI Appendix*, Text 5 and Table S1. The simulations were carried out for >2,000 y and are equilibrated in terms of temperature trends, energy balance, and overturning circulation. The NCAR CESM1.0 is a freely available model supported by the NSF and the Department of Energy.

We also use simulation outputs available from the BRIDGE portal as described in ref. 60. Some simulations were carried out for >8,000 y.

Data Availability. All proxy data generated or analyzed during this study are included in the *SI Appendix* files. Proxy data generated have also been deposited in the Purdue University Research Repository (doi: 10.4231/SFX6-RZ18) and at https://www.pangaea.de/. The model outputs, including netcdf files and source code for model data comparison, are available from M.H. (huberm@purdue.edu) and are permanently accessible at the Purdue University Research Repository.

All study data are included in the article and supporting information and/or are publicly accessible at the Purdue University Research Repository.

ACKNOWLEDGMENTS. C.L.O. acknowledges the support of a Yale Institute for Biospheric Studies Donnelley Postdoctoral Environmental Fellowship and NSF Award 1602557. This work was funded by an NSF grant to M.P., P.M.H., and M.H. (Awards OCE 1602557 and 1602905). We thank the International Ocean Discovery Program for providing samples for this study. We thank undergraduate laboratory assistants, E. Lazo-Wasem, H. J. Kim, and M. Kumera, for their help with sample preparation and M. Shankle for computing paleorotations using GPlates. We thank P. Markwick for providing late Oligocene paleogeographies and D. Evans, J. Hartman, R. Levy, Z. Lui, J. Plancq, and N. Sheldon for providing paleotemperature data. We thank A. Kennedy-Asser for making the UK model output available and D. Lunt for providing detailed instructions on how to analyze it. We thank D. Hutchinson for making GDFL CM2.1 model results for the late Eocene available. We thank M. Cramwinckel for helpful discussions regarding data handling in Fig. 3, C. Lear for advice regarding estimating Mg/Ca bottom water temperatures, E. Gasson for providing estimates of Oligocene ice volume, D. Colwyn for helpful discussions regarding terrestrial temperature proxy reconstructions, N. Herold and A. Goldner for conducting the initial paleoclimate simulations, and G. Foster for providing inspiration for this work. This manuscript was greatly improved by constructive feedback from the handling editor and four anonymous reviewers.

1. J. C. Zachos, G. R. Dickens, R. E. Zeebe, An early Cenozoic perspective on greenhouse warming and carbon-cycle dynamics. *Nature* **451**, 279–283 (2008).
2. C. H. Lear, T. R. Bailey, P. N. Pearson, H. K. Coxall, Y. Rosenthal, Cooling and ice growth across the Eocene–Oligocene transition. *Geology* **36**, 251–254 (2008).
3. K. G. Miller, J. D. Wright, R. G. Fairbanks, Unlocking the ice house: Oligocene–Miocene oxygen isotopes, eustasy, and margin erosion. *J. Geophys. Res. Solid Earth* **96**, 6829–6848 (1991).
4. J. V. Browning, K. G. Miller, D. K. Pak, Global implications of lower to middle Eocene sequence boundaries on the New Jersey coastal plain: The icehouse cometh. *Geology* **24**, 639–642 (1996).
5. D. Liebrand *et al*., Evolution of the early Antarctic ice ages. *Proc. Natl. Acad. Sci. U.S.A.* **114**, 3867–3872 (2017).
6. H. Pälike *et al*., The heartbeat of the Oligocene climate system. *Science* **314**, 1894–1898 (2006).
7. B. Cramer, K. Miller, P. Barrett, J. Wright, Late Cretaceous–Neogene trends in deep ocean temperature and continental ice volume: Reconciling records of benthic foraminiferal geochemistry ($\delta^{18}O$ and Mg/Ca) with sea level history. *J. Geophys. Res.* **116**, C12023 (2011).
8. C. H. Lear, Y. Rosenthal, H. K. Coxall, P. Wilson, Late Eocene to early Miocene ice sheet dynamics and the global carbon cycle. *Paleoceanography* **19**, PA4015 (2004).
9. D. Persico, G. Villa, Eocene–Oligocene calcareous nannofossils from Maud Rise and Kerguelen Plateau (Antarctica): Paleoecological and paleoceanographic implications. *Mar. Micropaleontol.* **52**, 153–179 (2004).
10. G. Villa, D. Persico, Late Oligocene climatic changes: Evidence from calcareous nannofossils at Kerguelen Plateau site 748 (Southern Ocean). *Palaeogeogr. Palaeoclimatol. Palaeoecol.* **231**, 110–119 (2006).
11. E. De Man, S. Van Simaeys, Late Oligocene warming event in the southern North Sea basin: Benthic foraminifera as paleotemperature proxies. *Neth. J. Geosci.* **83**, 227–239 (2004).
12. L. Alegret *et al*., Effects of the Oligocene climatic events on the foraminiferal record from Fuente Caldera section (Spain, western Tethys). *Palaeogeogr. Palaeoclimatol. Palaeoecol.* **269**, 94–102 (2008).
13. J. P. Kennett, Cenozoic evolution of Antarctic glaciation, the circum-Antarctic Ocean, and their impact on global paleoceanography. *J. Geophys. Res.* **82**, 3843–3860 (1977).
14. B. S. Cramer, J. R. Toggweiler, J. D. Wright, M. E. Katz, K. G. Miller, Ocean overturning since the Late Cretaceous: Inferences from a new benthic foraminiferal isotope compilation. *Paleoceanography* **24**, PA4216 (2009).
15. A. Goldner, N. Herold, M. Huber, Antarctic glaciation caused ocean circulation changes at the Eocene–Oligocene transition. *Nature* **511**, 574–577 (2014).
16. G. N. Inglis *et al*., Descent towards the Icehouse: Eocene sea surface cooling inferred from GDGT distributions. *Paleoceanography* **29**, 1000–1020 (2015).
17. M. E. Katz *et al*., Impact of Antarctic circumpolar current development on late Paleogene ocean structure. *Science* **332**, 1076–1079 (2011).
18. M. E. Katz *et al*., Stepwise transition from the Eocene greenhouse to the Oligocene icehouse. *Nat. Geosci.* **1**, 329–334 (2008).
19. Z. Zhang *et al*., Tropical seaways played a more important role than high latitude seaways in Cenozoic cooling. *Clim. Past* **7**, 801–813 (2011).
20. W. P. Sijp, M. H. England, M. Huber, Effect of the deepening of the Tasman gateway on the global ocean. *Paleoceanography* **26**, PA4207 (2011).
21. D. K. Hutchinson *et al*., Arctic closure as a trigger for Atlantic overturning at the Eocene–Oligocene transition. *Nat. Commun.* **10**, 3797 (2019).
22. D. J. Lunt *et al*., Palaeogeographic controls on climate and proxy interpretation. *Clim. Past* **12**, 1181–1198 (2016).
23. M. J. Cramwinckel *et al*., Synchronous tropical and polar temperature evolution in the Eocene. *Nature* **559**, 382–386 (2018).
24. E. Anagnostou *et al*., Changing atmospheric CO_2 concentration was the primary driver of early Cenozoic climate. *Nature* **533**, 380–384 (2016).
25. M. Pagani *et al*., The role of carbon dioxide during the onset of Antarctic glaciation. *Science* **334**, 1261–1264 (2011).
26. Y. G. Zhang, M. Pagani, Z. Liu, S. M. Bohaty, R. Deconto, A 40-million-year history of atmospheric CO_2. *Philos. Trans. A Math. Phys. Eng. Sci.* **371**, 20130096 (2013).
27. P. N. Pearson, G. L. Foster, B. S. Wade, Atmospheric carbon dioxide through the Eocene–Oligocene climate transition. *Nature* **461**, 1110–1113 (2009).
28. R. M. DeConto, D. Pollard, Rapid Cenozoic glaciation of Antarctica induced by declining atmospheric CO_2. *Nature* **421**, 245–249 (2003).
29. H. K. Coxall, P. A. Wilson, H. Pälike, C. H. Lear, J. Backman, Rapid stepwise onset of Antarctic glaciation and deeper calcite compensation in the Pacific Ocean. *Nature* **433**, 53–57 (2005).
30. G. L. Foster, D. L. Royer, D. J. Lunt, Future climate forcing potentially without precedent in the last 420 million years. *Nat. Commun.* **8**, 14845 (2017).
31. M. Tremblin, M. Hermoso, F. Minoletti, Equatorial heat accumulation as a long-term trigger of permanent Antarctic ice sheets during the Cenozoic. *Proc. Natl. Acad. Sci. U.S.A.* **113**, 11782–11787 (2016).
32. T. Tesfamichael *et al*., Settling the issue of "decoupling" between atmospheric carbon dioxide and global temperature $[CO_2]_{atm}$ reconstructions across the warming Paleogene–Neogene divide. *Geology* **45**, 999–1002 (2017).
33. R. Greenop *et al*., Orbital forcing, ice-volume and CO_2 across the Oligocene–Miocene transition. *Paleoceanogr. Paleoclimatol.* **34**, 316–328 (2019).
34. J. R. Super *et al*., North Atlantic temperature and pCO_2 coupling in the early-middle Miocene. *Geology* **46**, 519–522 (2018).
35. M. Steinthorsdottir *et al*., Fossil plant stomata indicate decreasing atmospheric CO_2 prior to the Eocene–Oligocene boundary. *Clim. Past* **12**, 439–454 (2016).
36. M. Steinthorsdottir, V. Vajda, M. Pole, Significant transient pCO_2 perturbation at the New Zealand Oligocene–Miocene transition recorded by fossil plant stomata. *Palaeogeogr. Palaeoclimatol. Palaeoecol.* **515**, 152–161 (2019).
37. L. Londoño *et al*., Early Miocene CO_2 estimates from a Neotropical fossil leaf assemblage exceed 400 ppm. *Am. J. Bot.* **105**, 1929–1937 (2018).
38. S. F. Pekar, R. M. DeConto, D. M. Harwood, Resolving a late Oligocene conundrum: Deep-sea warming and Antarctic glaciation. *Palaeogeogr. Palaeoclimatol. Palaeoecol.* **231**, 29–40 (2006).
39. J. D. Hartman *et al*., Paleoceanography and ice sheet variability offshore Wilkes Land, Antarctica—Part 3: Insights from Oligocene–Miocene TEX_{86}-based sea surface temperature reconstructions. *Clim. Past* **14**, 1275–1297 (2018).
40. Z. Liu *et al*., Global cooling during the Eocene–Oligocene climate transition. *Science* **323**, 1187–1190 (2009).
41. B. S. Wade *et al*., Multiproxy record of abrupt sea-surface cooling across the Eocene–Oligocene transition in the Gulf of Mexico. *Geology* **40**, 159–162 (2012).
42. J. Hansen, M. Sato, G. Russell, P. Kharecha, Climate sensitivity, sea level and atmospheric carbon dioxide. *Philos. Trans. A Math. Phys. Eng. Sci.* **371**, 20120294 (2013).
43. P. N. Pearson *et al*., Warm tropical sea surface temperatures in the Late Cretaceous and Eocene epochs. *Nature* **413**, 481–487 (2001).
44. P. N. Pearson *et al*., Stable warm tropical climate through the Eocene Epoch. *Geology* **35**, 211–214 (2007).
45. P. J. Markwick, "The palaeogeographic and palaeoclimatic significance of climate proxies for data-model comparisons" in *Deep-Time Perspectives on Climate Change: Marrying the Signal from Computer Models and Biological Proxies*, M. Williams, A. Haywood, F. Gregory, D. Schmidt, Eds. (The Micropalaeontology Society and The Geological Society of London, London, 2007), pp. 251–312.
46. Z. Liu *et al*., Transient temperature asymmetry between hemispheres in the Palaeogene Atlantic Ocean. *Nat. Geosci.* **11**, 650–656 (2018).
47. J. E. Tierney, M. P. Tingley, A. Bayesian, Spatially-varying calibration model for the TEX_{86} proxy. *Geochim. Cosmochim. Acta* **127**, 83–106 (2014).
48. J. E. Tierney, M. P. Tingley, A TEX_{86} surface sediment database and extended Bayesian calibration. *Sci. Data* **2**, 150029 (2015).
49. S. Schouten, E. C. Hopmans, E. Schefuß, J. S. Sinninghe Damsté, Distributional variations in marine crenarchaeotal membrane lipids: A new tool for reconstructing ancient sea water temperatures? *Earth Planet. Sci. Lett.* **204**, 265–274 (2002).
50. S. Petersen, D. Schrag, Antarctic ice growth before and after the Eocene–Oligocene transition: New estimates from clumped isotope paleothermometry. *Paleoceanogr. Paleoclimatol.* **30**, 1305–1317 (2015).
51. P. M. J. Douglas *et al*., Pronounced zonal heterogeneity in Eocene southern high-latitude sea surface temperatures. *Proc. Natl. Acad. Sci. U.S.A.* **111**, 6582–6587 (2014).
52. J. Plancq, E. Mattioli, B. Pittet, L. Simon, V. Grossi, Productivity and sea-surface temperature changes recorded during the late Eocene–early Oligocene at DSDP site 511 (South Atlantic). *Palaeogeogr. Palaeoclimatol. Palaeoecol.* **407**, 34–44 (2014).
53. B. R. Hines *et al*., Reduction of oceanic temperature gradients in the early Eocene southwest Pacific Ocean. *Palaeogeogr. Palaeoclimatol. Palaeoecol.* **475**, 41–54 (2017).
54. P. K. Bijl *et al*., Transient middle Eocene atmospheric CO_2 and temperature variations. *Science* **330**, 819–821 (2010).
55. C. H. Lear, H. Elderfield, P. A. Wilson, Cenozoic deep-sea temperatures and global ice volumes from Mg/Ca in benthic foraminiferal calcite. *Science* **287**, 269–272 (2000).

56. C. F. Dawber, A. K. Tripati, Constraints on glaciation in the middle Eocene (46–37 Ma) from Ocean Drilling Program (ODP) site 1209 in the tropical Pacific Ocean. *Paleoceanography* **26**, PA2208 (2011).
57. Y. G. Zhang, M. Pagani, Z. Wang, Ring index: A new strategy to evaluate the integrity of TEX_{86} paleothermometry. *Paleoceanography* **31**, 220–232 (2016).
58. D. De Vleeschouwer, M. Vahlenkamp, M. Crucifix, H. Pälike, Alternating Southern and Northern Hemisphere climate response to astronomical forcing during the past 35 my. *Geology* **45**, 375–378 (2017).
59. J. S. Eldrett, D. R. Greenwood, I. C. Harding, M. Huber, Increased seasonality through the Eocene to Oligocene transition in northern high latitudes. *Nature* **459**, 969–973 (2009).
60. A. T. Kennedy-Asser *et al*., Changes in the high latitude Southern Hemisphere through the Eocene–Oligocene transition: A model-data comparison. *Clim. Past* **16**, 555–573 (2020).
61. D. J. Lunt *et al*., A model–data comparison for a multi-model ensemble of early Eocene atmosphere–ocean simulations: EoMIP. *Clim. Past* **8**, 1717–1736 (2012).
62. D. Tardif *et al*., The origin of Asian monsoons: A modelling perspective. *Clim. Past* **16**, 847–865 (2020).
63. A. Goldner, N. Herold, M. Huber, The challenge of simulating the warmth of the mid-Miocene climatic optimum in CESM1. *Clim. Past* **10**, 523–536 (2014).
64. J. Zhu, C. J. Poulsen, J. E. Tierney, Simulation of Eocene extreme warmth and high climate sensitivity through cloud feedbacks. *Sci. Adv.* **5**, eaax1874 (2019).
65. N. J. Burls, A. V. Fedorov, Wetter subtropics in a warmer world: Contrasting past and future hydrological cycles. *Proc. Natl. Acad. Sci. U.S.A.* **114**, 12888–12893 (2017).
66. J. E. Tierney, A. M. Haywood, R. Feng, T. Bhattacharya, B. L. Otto-Bliesner, Pliocene warmth consistent with greenhouse gas forcing. *Geophys. Res. Lett.* **46**, 9136–9144 (2019).
67. D. K. Hutchinson *et al*., Climate sensitivity and meridional overturning circulation in the late Eocene using GFDL CM2. 1. *Clim. Past* **14**, 789–810 (2018).
68. R. Caballero, M. Huber, State-dependent climate sensitivity in past warm climates and its implications for future climate projections. *Proc. Natl. Acad. Sci. U.S.A.* **110**, 14162–14167 (2013).
69. K. D. Burke *et al*., Pliocene and Eocene provide best analogs for near-future climates. *Proc. Natl. Acad. Sci. U.S.A.* **115**, 13288–13293 (2018).
70. D. L. Royer, Climate sensitivity in the geologic past. *Annu. Rev. Earth Planet. Sci.* **44**, 277–293 (2016).
71. D. Pollard, R. M. DeConto, Hysteresis in Cenozoic Antarctic ice-sheet variations. *Global Planet. Change* **45**, 9–21 (2005).
72. G. J. Paxman *et al*., Reconstructions of Antarctic topography since the Eocene–Oligocene boundary. *Palaeogeogr. Palaeoclimatol. Palaeoecol.* **535**, 109346 (2019).
73. G. Knorr, G. Lohmann, Climate warming during Antarctic ice sheet expansion at the Middle Miocene transition. *Nat. Geosci.* **7**, 376 (2014).
74. A. T. Kennedy, A. Farnsworth, D. J. Lunt, C. H. Lear, P. J. Markwick, Atmospheric and oceanic impacts of Antarctic glaciation across the Eocene–Oligocene transition. *Philos. Trans. A Math. Phys. Eng. Sci.* **373**, 20140419 (2015).
75. A. Goldner, M. Huber, R. Caballero, Does Antarctic glaciation cool the world? *Clim. Past* **9**, 173–189 (2013).
76. C. J. Hollis *et al*., Early Paleogene temperature history of the southwest Pacific Ocean: Reconciling proxies and models. *Earth Planet. Sci. Lett.* **349**, 53–66 (2012).
77. C. E. Stickley *et al*., Timing and nature of the deepening of the Tasmanian Gateway. *Paleoceanography* **19**, PA4027 (2004).
78. P. K. Bijl *et al*., Early Palaeogene temperature evolution of the southwest Pacific Ocean. *Nature* **461**, 776–779 (2009).
79. P. K. Bijl *et al*.; Expedition 318 Scientists, Eocene cooling linked to early flow across the Tasmanian Gateway. *Proc. Natl. Acad. Sci. U.S.A.* **110**, 9645–9650 (2013).
80. P. F. Barker, J. Burrell, The opening of Drake passage. *Mar. Geol.* **25**, 15–34 (1977).
81. F. R. Rack, A geologic perspective on the Miocene evolution of the Antarctic circumpolar current system. *Tectonophysics* **222**, 397–415 (1993).
82. T. Herbert, Into the Ice Age. *Nat. Geosci.* **11**, 624–625 (2018).
83. C. Lyell, *Principles of Geology: Being An Inquiry How Far the Former Changes of the Earth's Surface Are Referable to Causes Now in Operation*, (John Murray, London, 1833), Vol. vol. 3.
84. F. M. Gradstein, J. G. Ogg, M. D. Schmitz, G. M. Ogg, *The Geologic Time Scale 2012*, (Elsevier, 2012), Vol. vol. 2.
85. K. J. Matthews *et al*., Global plate boundary evolution and kinematics since the late Paleozoic. *Global Planet. Change* **146**, 226–250 (2016).
86. F. Florindo *et al*., New magnetobiostratigraphic chronology and paleoceanographic changes across the Oligocene-Miocene boundary at DSDP site 516 (Rio Grande Rise, SW Atlantic). *Paleoceanogr. Paleoclimatol.* **30**, 659–681 (2015).
87. R. Gennari *et al*., High-resolution integrated calcareous plankton biostratigraphy and magnetostratigraphy at the Oligocene–Miocene transition in southwestern Atlantic Ocean. *Geol. J.* **53**, 1079–1101 (2018).
88. J. Hess, L. D. Stott, M. L. Bender, J. P. Kennett, J. G. Schilling, The Oligocene marine microfossil record: Age assessments using strontium isotopes. *Paleoceanography* **4**, 655–679 (1989).
89. S. Schouten, C. Huguet, E. C. Hopmans, M. V. Kienhuis, J. S. Damsté, Analytical methodology for TEX_{86} paleothermometry by high-performance liquid chromatography/atmospheric pressure chemical ionization-mass spectrometry. *Anal. Chem.* **79**, 2940–2944 (2007).
90. E. C. Hopmans, S. Schouten, J. S. S. Damsté, The effect of improved chromatography on GDGT-based palaeoproxies. *Org. Geochem.* **93**, 1–6 (2016).
91. E. C. Hopmans *et al*., A novel proxy for terrestrial organic matter in sediments based on branched and isoprenoid tetraether lipids. *Earth Planet. Sci. Lett.* **224**, 107–116 (2004).
92. Y. G. Zhang *et al*., Methane index: A tetraether archaeal lipid biomarker indicator for detecting the instability of marine gas hydrates. *Earth Planet. Sci. Lett.* **307**, 525–534 (2011).
93. N. Herold, M. Huber, R. Müller, M. Seton, Modeling the Miocene climatic optimum: Ocean circulation. *Paleoceanography* **27**, PA1209 (2012).
94. H. Zhou, B. R. Helliker, M. Huber, A. Dicks, E. Akçay, C_4 photosynthesis and climate through the lens of optimality. *Proc. Natl. Acad. Sci. U.S.A.* **115**, 12057–12062 (2018).
95. A. Hossain, G. Knorr, G. Lohmann, M. Stärz, W. Jokat, Simulated thermohaline fingerprints in response to different Greenland-Scotland Ridge and Fram Strait subsidence histories. *Paleoceanogr. Paleoclimatol.* **35**, e2019PA003842 (2020).